# Galaxy Morphology Through Texture Analysis

Kinman Au

PhD Thesis Proposal

## 1 Introduction

Galaxy Morphology is the study of how a galaxy form its shape and how the morphology relates to its evolutionary history. The goal of my thesis is to derive a quantitative, rich, and physically meaningful description of galaxy morphology, particularly, the description of **bar** and **spiral** structure of a galaxy, so that astronomers can study, with much higher efficiency and accuracy, the relationship between the morphological properties of galaxies and the local environment with which they interact, such as local density of galaxies, and other features of galaxies, such as redshift. We will gain insight into how galaxies evolve by investigating such relationships.

Modern studies of galaxy morphology began in 1920's when Edwin Hubble, based on his observation of galaxies, proposed a classification scheme. (see section 2.1). He tried to relate a galaxy's morphological type to its evolutionary stage, but his proposed relationship is now believed to be wrong. Nevertheless, the attempt to understand the evolutionary history of galaxies from their morphology has continued .

Recent advances in telescope and theory of galaxy evolution have given new momentum to the research in galaxy morphology. The Hubble Space Telescope has taken very deep snapshots of the sky, revealing galaxies down to unprecedentedly faint levels. Meanwhile, new hypothesis on Dark Matter opens a new door to understand the evolution of galaxies and the Universe. (see section 2). In addition, the modern large scale sky surveys like Sloan Digital Sky Survey (SDSS), have been producing enormous number of galaxy images along with other data which allow cosmologists to study the evolutionary history of galaxies.

A main problem in studying galaxy morphology is that we do not have an objective and quantitative description of morphological properties. Hubble's scheme and its extensions are subjective. Apart from their imprecision in categorizing galaxies, it is also not suitable for study enormous amount of digital images from the modern sky surveys. Hence a quantitative scheme is needed to conduct research on galaxy morphology. There are attempts to describe Galaxy images using different measures, like Bulge-to-Disk ratio and Principal Components. (see section 2.2) which however cannot give sufficiently rich description of galaxy morphology, e.g. they cannot distinct subcategories of spiral structure.

This work describes a new approach for characterization of galaxy images. By studying the **textural** properties of them, we can extract features that could well characterize spiral and bar structure in galaxy images. Another advantage of this approach is that we can study the local structure of galaxy images at different scales.

# 2 Scientific Background and Motivation

Understanding the formation and subsequent evolution of galaxies is a central issue of astronomy. Modern studies on galaxy evolution and morphology began in 1920's when Hubble proposed his famous galaxy classification scheme (see section 2.1) and has become an active active research area in astronomy. Recently, the advances in both theory of galaxy evolution and observation technology have given new momentum to the research of galaxy morphology.

Under the modern theory of galaxy evolution, early galaxies (high redshift) were mostly in disk shape, before evolving into spirals. In addition to such isolated transformation, interaction among galaxies, through collision and merging (depends on the local density of galaxies), creates elliptical galaxies, see Figure19. By investigating how distribution of morphological type related to variables like redshift or local density of galaxies, we will be able to verify and gain insight to the theory.

Another driving force of modern research of galaxy morphology is the latest technology. Hubble Space Telescope (HST) can now capture large amount of well resolved images of very distant objects (high redshift). It is also a main impulse for development of quantitative morphology scheme that can deal with large amount of emerging new data.

## 2.1 Hubble Scheme

Edwin Hubble introduced the morphological classification scheme in 1920s for galaxies still in use today. In his "tuning fork" diagram, galaxies are divided into three major types : ellipticals, spirals and irregular (see figure). Elliptical galaxies are smooth featureless, almost spherical systems. Spiral galaxies, such as our own Milky Way, are flatted and organized structures in which stars and gas move on circular or near-circular orbits around the center. Irregular (Irr) galaxies is a catch-all category for those do not fit into elliptical and spiral.

Hubble's scheme subdivided spiral galaxies into unbarred(S) and barred(SB) categories, which define the times of the tuning fork. Along each tine, galaxies are further subdivided according to the tightness of their spiral arms, which changes monotonically along the tuning fork, in step with fraction of light in the central bulge of the galaxy. Theses subcategories are denoted Sa, Sb and Sc(SBa, SBb,SBc in the case of barred spirals).

Though Hubble's scheme attempts to classify galaxies according to their appearance, Hubble also offer an insight into the physical origin of the different types. He refereed to the Sb, Sc and Irr

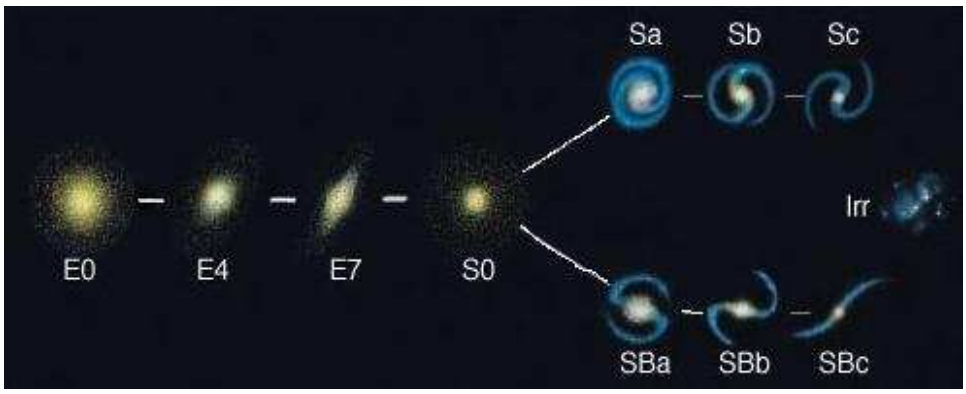


Figure 1: Hubble Scheme - commonly known as Hubble Turning Fork. This tuning-fork diagram divides galaxies into elliptical (E's) and spirals (S's). A third group is formed by the irregulars (Irr's). Elliptical galaxies have the shape of an ellipsoid. The S0 galaxies or lenticular galaxies are midway between ellipticals and spirals, they have a nuclear bulge surrounded by a flat disk, but no spiral arms. There are two kinds of spiral galaxies, normal and barred. Sa, Sb, Sc for normal spirals, SBa, SBb, Sbc for barred spirals.

types as '"late type galaxies" and the ellipticals and S0s as "early types", imagining an evolutionary sequence along the tuning fork.

Though Hubble's scheme is still a popular classification system, it is not adequate for modern galaxy morphology research. Instead, a quantitative approach to galaxy morphology is needed to deal with the new data.

### 2.2 Quantitative Approach to Galaxy Morphology

The subjective nature of Hubble scheme and it's extensions brings taxonomical inexactitude. Moreover, such a scheme is inadequate to process massive amount of data generated from modern sky survey. These are the major reason for the development of computer-based objective classification schemes based on the measurement of quantitative parameters. However, so there are no objective scheme that can emcompass the full richness of galaxy forms. For example, no quantitative scheme can currently distinguish between physically distinct subcategories of spiral structure.

**Bulge-to-Disk ratio** [4] is arguably the most popular quantitative characterization of galaxies images nowadays. By decomposing a galaxy image into central high brightness component (Bulge) and periphery dimer component (Disk), we can estimate the weight of each component. As along the Hubble sequence, from early-type to late type, the bulge-to-disk ratio decrease, astronomers can hence related Bulge-to-Disk ratio with Hubble types. It explains why it gain such a popularity among astronomers.

Another approach to analyze galaxy images by projecting images into a set of basis functions. One popular basis is Eigenbasis or **Principal Component basis** [11], however Principal Component fails represent the local structure in a image, like spiral or bar.

# 3 Texture Analysis for extracting morphological features

My thesis proposes an alternate approach to represent and analyze galaxy images by studying their textural property. Texture analysis is vast field in computer vision which studies the local neighborhood properties of the gray levels of an image region. There are numerous schemes to study texture of an image [12]. In my thesis, I use wavelet style analysis (multiscale, localized) to study the orientation of texture. Orientation analysis is an important task in computer vision [7]. By estimating the strength and direction of orientation for each pixel, we have a low level representation of an galaxy image which enable us to extract high level description such as 'barness' and 'spiral-ness'.

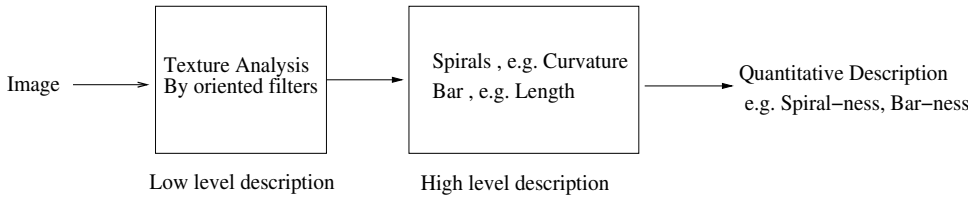


Figure 2: Schematic diagram for characterization and classification of galaxy images

## 3.1 Orientation Analysis

This section gives a basic idea of orientation analysis of monoscale image texture. Multiscale analysis is discussed in next section. We delay the description of the implementation details to section 5.1

The first step of (monoscale) orientation analysis is to convolve an image with a set of oriented filters. Figure 3 shows a set of nine filters used in the analysis . As a result for each image we can obtain nine images after the convolution (Figure 4). We can then estimate the strength and direction of orientation for every location of the image (Figure 5).

## 3.2 Multiscale Analysis

The local structure of a image has various degree of coarseness, therefore we need to perform orientation analysis in a multiscale setting. The analysis consists of two stages : (1) Extract

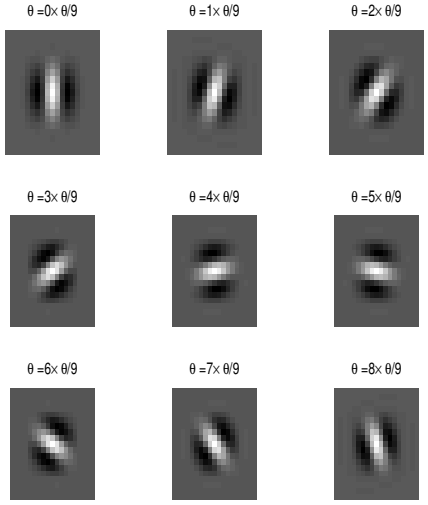


Figure 3: Images of oriented filters at nine different angles.

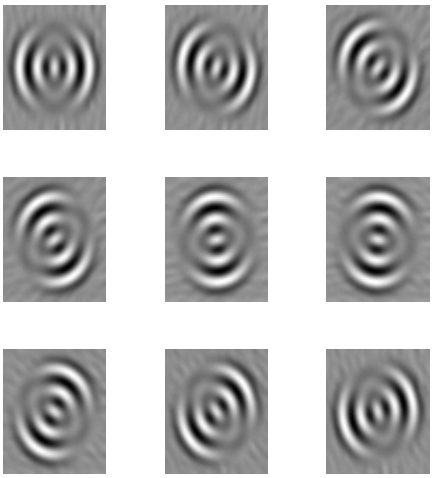

Figure 4: Cosine Wave images (figure 5) convolved with nine oriented filters depicted in figure 3

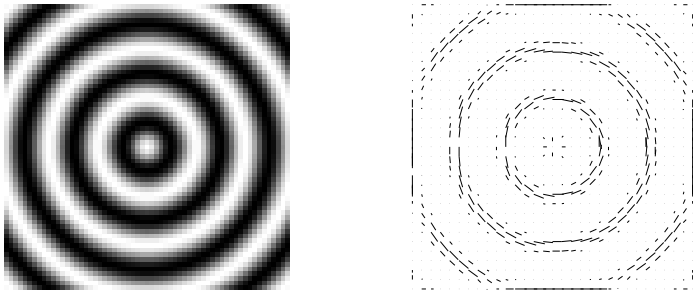

Figure 5: Left:(a) A 2D image of cosine wave. Right:(b) Orientation field of cosine wave. Each rod on the plot shows the orientation of the wave at that location and the length represents strength of orientation.

orientation information at different scales using a pyramid algorithm, (2) Combine information from all scales.

### 3.2.1 Extract information from different scales.

Pyramid algorithm is a common tool to encode and extract multiscale information. In this thesis, I derive a pyramid algorithm which incorporates the orientation filters described in previous section. This algorithm enable us to analyze orientation structure of an image under different scale.

Section 5.3 describes the details of the algorithm. And Figure 7 is an example showing how to extract orientation information under a multiscale setting using such algorithm.

In general, we have a smooth flow of orientation field under coarse scale but with loss of detail structure. On the other hand, under fine scale detail structure can be capture but with more noise. We need to combine information from all scales to obtain better estimation.

### 3.2.2 Combine Multiscale Information

Section 5.5 describes an algorithm that combines orientation information from all scales. It is done by updating an orientation field, starting from the coarsest scale, by another orientation field of next finer scale, iteratively. Figure 8 and 9 give examples of such updating.

Figure 6: 2D Doppler function

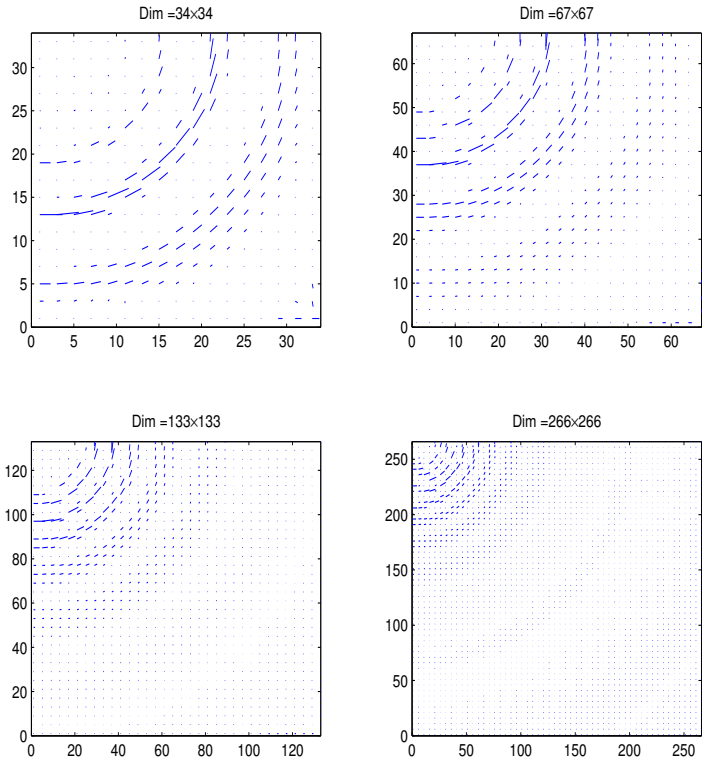


Figure 7: Orientation field of 2D Doppler function at different scales. The dimensions of the images go from $200 \times 200$ for the fine scale to $25 \times 25$ for coarse scale.

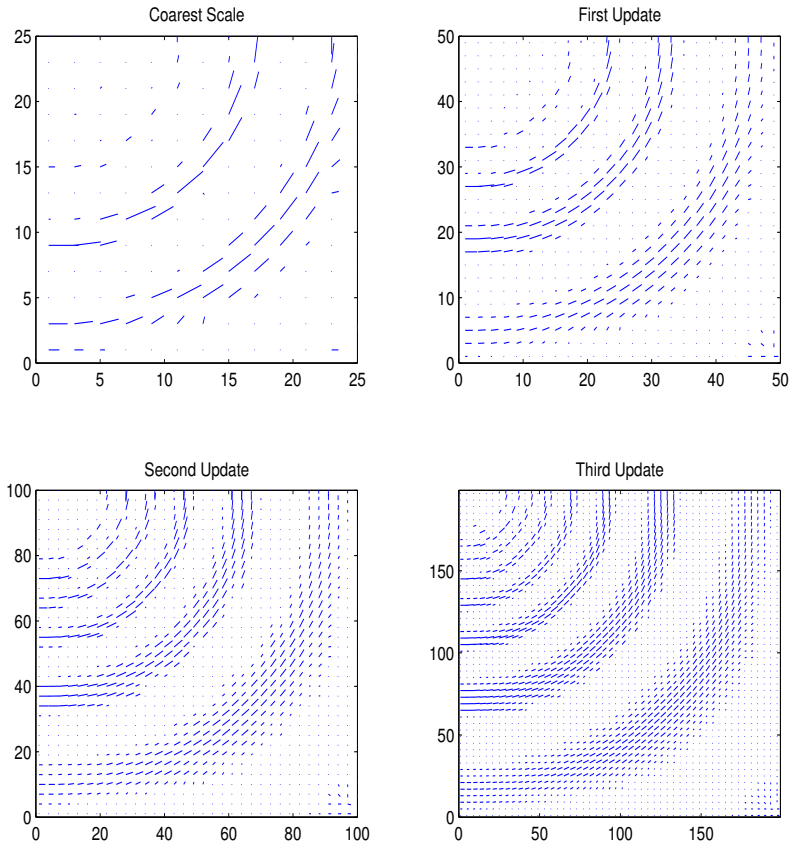


Figure 8: Merging of orientation field for 2D Doppler function from all scales. Starting from the coarsest scale. Orientation information is updated by adding details from next finer scale.

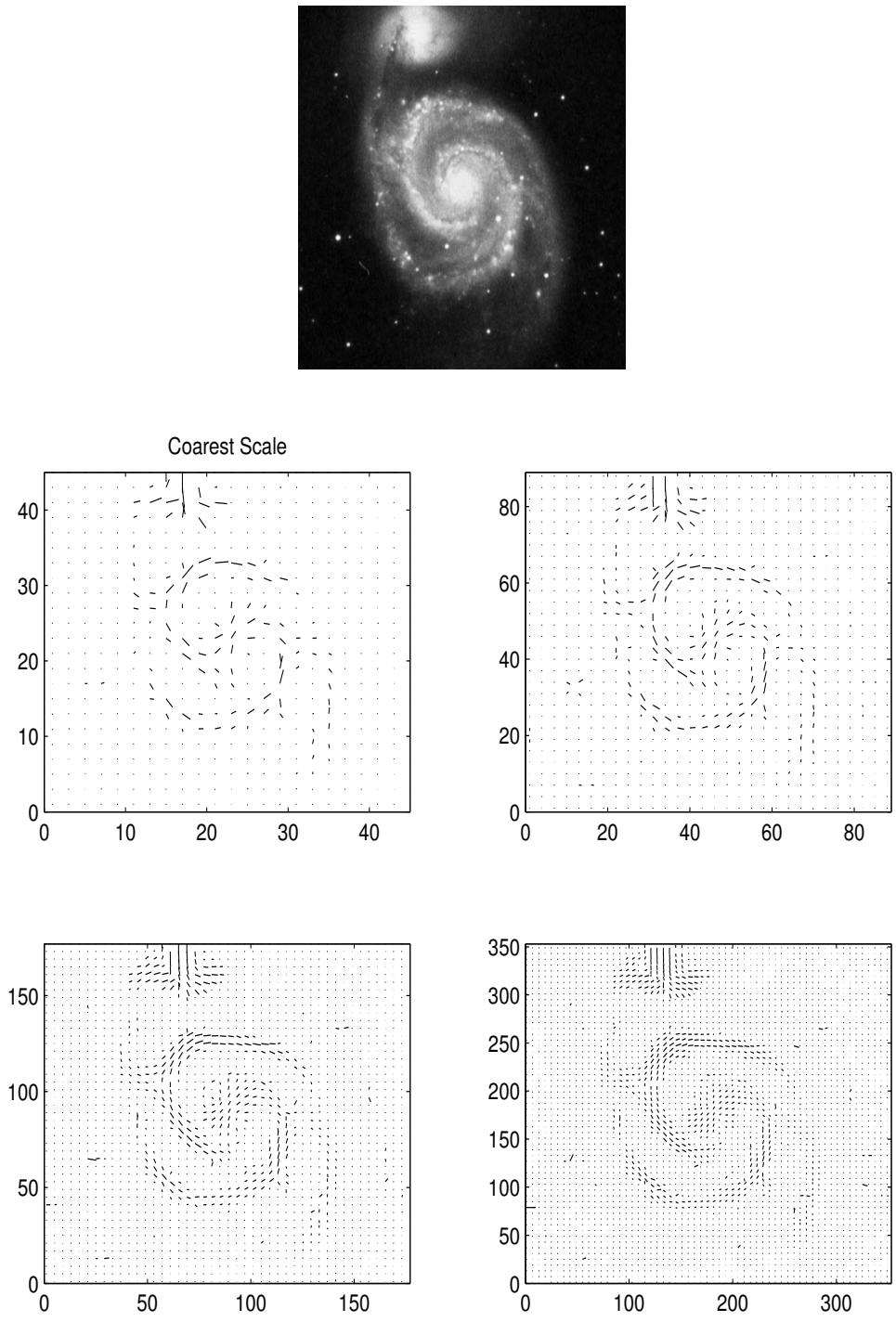


Figure 9: Merging orientation field for M51 image from all scales.

## 4 Measures for Bar-ness

Based on the orientation field, we can derive measures of bar-ness by fitting a rectangle to structure at the center of a image that has homogeneous orientation. Figure 10 shows fitted rectangle to a set of spiral galaxies with bar structure of different size, while Figure 11 shows elliptical galaxies and some edge-on galaxies without much surface textural. For face-on galaxies, we can see size of fitted rectangle of an barred galaxy is larger than the bulge(see Figure 20). Whereas, for a non-barred galaxy, the fitted rectangle is relatively smaller. Therefore rectangle-to-bulge ratio in size is a measure of bar-ness. Also, for an non-barred face-on galaxy, length-to-width ratio of the fitted rectangle is close to one. This ratio can be used as another measure of bar-ness.

For a edge-on galaxy, we cannot observe much textural feature on the surface and it is often that a rectangle would be fitted to the whole galaxy. And we need other features of the galaxy, such as size of the whole galaxy, ellipticity, spiral-ness, to decide if it is a real bar structure.

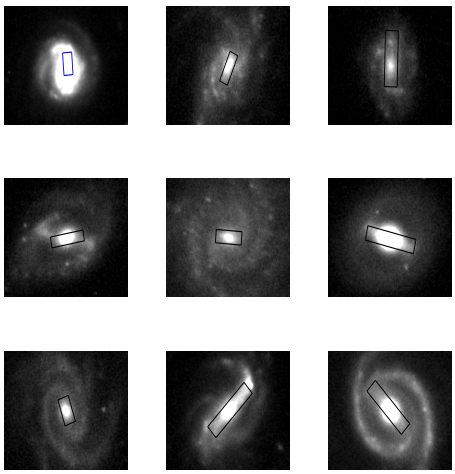

Figure 10: Spiral galaxies with fitted rectangles.

## 5 Discussion and Future Work

So far, I have implemented the algorithm for texture analysis. The algorithm extracts low level description of galaxy morphology. Mathematically, our orientation field can be represented as,

$$\frac{dy}{dx}|_{(x_i,y_i)} = F(x_i, y_i),$$

and each point is weighted by orientation strength.

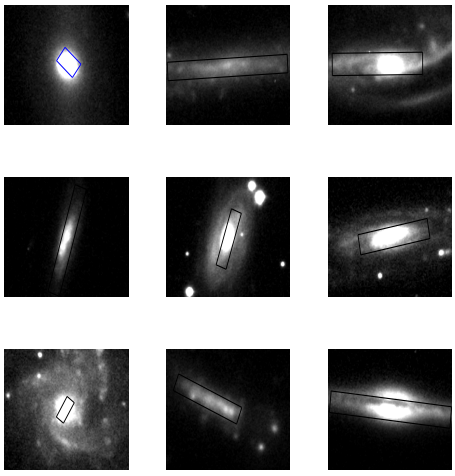

Figure 11: Elliptical galaxies, edge-on galaxies with fitted rectangles.

The next step of my work is to derive a high level description of the orientation field. A measure of bar-ness is proposed in Section 4. Another important feature I will study is the spiral-ness of a galaxy.

The ultimate objective of my work is to study how Galaxy Morphology is related to the evolutionary history. I plan to apply my algorithm to analyze real galaxy images. Images from Hubble Space Telescope(e.g. GOODS[1]) , ground telescopes (e.g. SDSS[2]) provide huge amount of data for such study.

The textural algorithm can be extended to study 3D data. One possible application of such extension is in the study of large-scale structure of the Universe. When we investigate the structure of the Universe in large scale (in a dimension of hundreds of million light years) ,the Universe exhibit a filament-like structure, see figure 12. Astrophysicists are interested in finding out whether there is a filament between two clusters of galaxies and what is its curvature if such a filament exist. This problem is similar to identification and characterization of spiral arms in galaxy.

[1]The Great Observatories Origins Deep Survey. http://www.stsci.edu/science/goods/

[2]Sloan Digital Sky Survey. http://www.sdss.org/

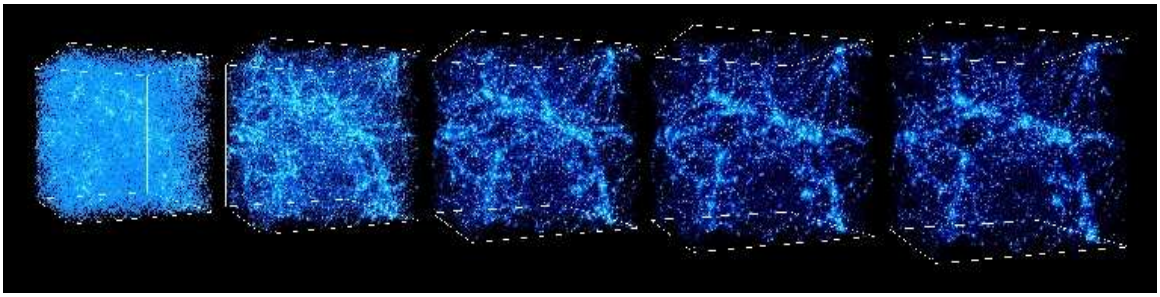

Figure 12: Simulation of the evolution of large scale structure of the universe.Pictures above the formation of clusters and large-scale filaments in the Cold Dark Matter model. The pictures show the evolution of structures in a 43 million parsecs (or 140 million light years) box from redshift of 30 to the present epoch (leftmost z=30 to rightmost z=0). The leftmost image represent distribution of matter at the early age of the Universe which appears to be uniform. This is because the seed fluctuations are still fairly small. As time goes on, the fluctuations grow resulting in a wealth of structures from the smallest bright clumps which have sizes and masses similar to those of galaxies to the large filaments. Result of Kravstsov [8]

## References


[1] P.J Burt and E. H. Adelson. Laplican pyramid as a compact image code. *IEEE Trans. Commun.*, 1983.

[2] E. J. Cands and D. L. Donoho. Ridgelets: a key to higher-dimensional intermittency? *Phil. Trans. R. Soc. Lond. A.*, 1999.

[3] I Daubechies. *Ten Lectures on Wavelets*. SIAM, 1992.

[4] L. Simard et al. The deep groth strip survey. ii. hubble space telescope structural parameters of galaxies in the groth strip. *The Astrophysical Journal*, 2002.

[5] J. T. Kent K. V. Mardia and J. M. Bibby. *Multivariate Analysis*. Academic Press, 1989.

[6] R. Nikoukhah K.C. Chou, A.S. Willsky. Multiscale systems, kalman filters, and riccati equations. *IEEE Transactions on Automatic Control, Vol.39, N0.3*, 1994.

[7] H. Knutsson and G. H. Granlund. Texture anlysis using two-dimensional quadrature filters. *IEEE Comuter Sociey Workshop on Computer Architecture for Pattern Analysis and Image Database Managment*, pages 206–213, 1983.

[8] Andrey Kravtsov and Anatoly Klypin. http://cosmicweb.uchicago.edu/index.html.

[9] K. V. Mardia and P. E.Jupp. *Directional Statistical*. John Wiley & Sons, 2000.

[10] Eero P Simoncelli and William T Freeman. The steerable pyramid: A flexible architecture for multi-scale derivative computation. *Proc 2nd IEEE Int'l Conf on Image Processing*, 1995.

[11] Gyula Szokoly. *Deep multicolor surveys of the galaxy population*. PhD thesis, Johns Hopkins University, 1999.

[12] M. Tuceryan and A. K. Jain. Texture analysis. *The Handbook of Pattern Recognition and Computer Vision*, 1998.

# APPENDIX

## 5.1 Textural Analysis Algorithm

### 5.1.1 Construction of oriented Filters

This section describes how to create a set of 2D oriented filters based on 1D Mexican Hat filter.

The Mexican hat function is the second derivative of the Gaussian $e^{-x^2/2}$; if we normalize it so that its $L^2$ norm is 1, we obtain

$$\phi(x) = 2/\sqrt{3}\pi^{-1/4}(1-x^2)e^{-x^2/2}.$$

(see Figure 21)

Let

$$\rho_r(X) = \phi(X^T r), \tag{1}$$

where $X = [x, y]^T$ and $r = [\cos(\theta), \sin(\theta)]^T$. Therefore $\rho_r(X)$ is a ridge function used in projection pursuit regression(see Figure 22). Candes and Donoho [2] uses ridge functions to create wavelet style signal approximation algorithm called Ridgelet. A problem with this construction is that the support of filters span across whole image along the orientation of $r$.

In order to localize $\rho_r(X)$ , I use windowed version of function $\rho_{\theta,r}(\cdot)$, i.e.

$$\psi_\theta(\mathbf{x}) = \rho(x, y) \times 1/\sqrt{2}e^{-1/2(x^2+y^2)}, \tag{2}$$

(see Figure 23) where $\mathbf{x} = (x, y)$.

## 5.2 Transformation and Estimation

A monoscale continuous Transform with $\phi$ is

$$(T^\psi f)(\theta, \mathbf{u}) = \int f(\mathbf{t})\psi_\theta(\mathbf{t}-\mathbf{u})d\mathbf{t}, \tag{3}$$

at point $\mathbf{u}$ ant angle $\theta$.

In digital image processing, we need to discretize the transform depicted by Eq(3). Rigorous analysis of discrete transform could be performed by using theory of frame [3].

Here we use a set of nine discrete filters, each with 11 taps for both dimension, oriented in 9 angles i.e. $i\frac{\pi}{9}, i = 0 \ldots 8$. Hence, the discretized transform (DT) of if a digitalized image (I) becomes

$$(DT^\psi I)(\theta) = I * \psi_\theta^D, \quad \theta = i\frac{\pi}{9}, i = 0 \ldots 8,$$

where $\psi_\theta^D$ is discretized version of $\psi_\theta$ and $*$ is the convolution operator.

I use the mean direction and strength of directionality ,[5], [9], of the energy of transform - square of the transform. Let

$$r = \sum_{\theta} (DT^{\psi} I)(\theta)^2 \exp(i * 2\theta)$$

, where $i = \sqrt{-1}$ and we use $2\theta$ (2-fold wrapping [9]) because $\theta$ and $-\theta$ are equivalent. And we can now define the angle of orientation $A(\mathbf{u})$ as

$$A(\mathbf{u}) = \arg(r)/2; \tag{4}$$

and strength of orientation $S(\mathbf{u})$ as

$$S(\mathbf{u}) = ||r|| \tag{5}$$

### 5.3 Pyramid Coding and Multiscale Analysis

A pyramid algorithm is a general term for data structures that condense information successively [1], [10]. It is useful in multiscale analysis of digital images.

Schematic diagram of the pyramid algorithm used in this work is shown in Figure 13. Initially, the image is separated into low and highpass subbands, using filters L0 and H0. The lowpass subband is then divided into a set of oriented bandpass subbands by passing through a set of oriented filters, and a low(er)-pass subband. This low(er)-pass subband is subsampled by a factor of 2 in the X and Y directions. The recursive (pyramid) construction of a pyramid is achieved by inserting a copy of the shaded portion of the diagram at the location of the solid circle (i.e., the lowpass branch). As a result, this algorithm decompose of an image into scale and orientation subbands, (figure 14) and we can hence estimate orientation strength and angle at different scales.

By applying a set of oriented filters at different level, we further partition the Fourier space into subbands at different orientation, see figure 13. As a result, we can estimate orientation strength and angle at different scales.

### 5.4 Comparison with Wavelet Transform

Wavelet pyramid uses only four filtering operations, they are

1. lowpass in both x and y axes.
2. lowpass in x and highpass in y.
3. lowpass in y and highpass in x.
4. highpass in both x and y.

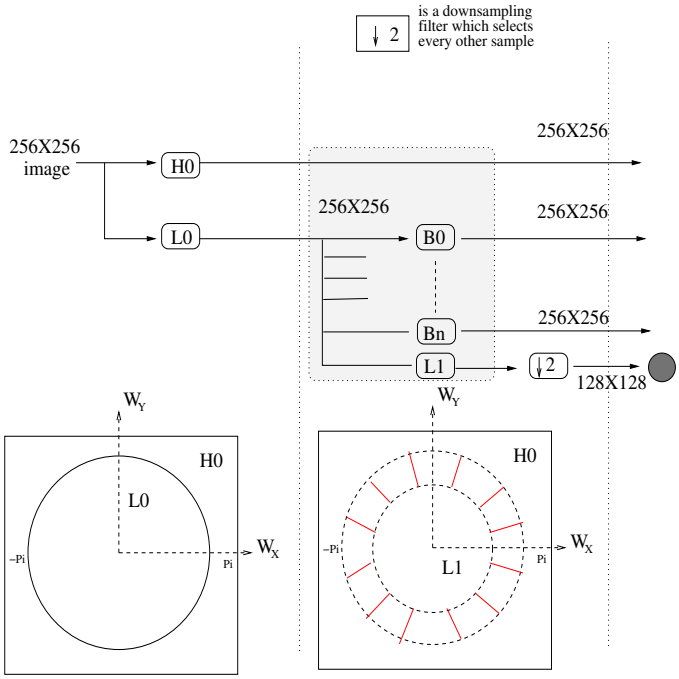


Figure 13: Schematic diagram of the pyramid algorithm for multiscale analysis.The first stage is the preprocessing that a image passes through a low/highpass filters $L0$. Lower left picture shows how such filters partition the Fourier domain. In next stage (the shaded part) oriented filters further partition the Fourier domain into angular slice - subbands of different direction (the lower right picture). The filled circle means repetition of the shaded part until the dimensions of the image is less than that of the filters.

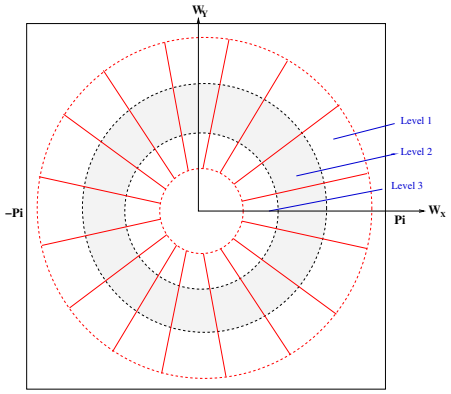


Figure 14: Idealized depiction of three-level pyramid algorithm in Fourier domain.

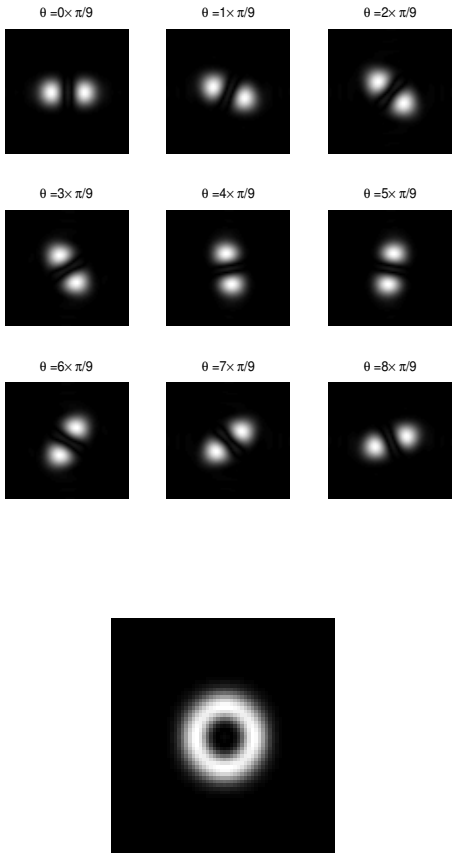


Figure 15: Top: Fourier Transform of nine oriented filters (see figure 3) after first stage lowpass filter (see figure 13) i.e. $\mathcal{F}(L0 * Bi), i = 0 \ldots 8$. Bottom: Annular Ring - Total spectral power of $L0 * B_i$.

As a result, wavelet transform has only three oriented basis functions - vertical, horizontal and both diagonal - a checkerboard pattern and the sum of spectral power of all the basis function is a square. Therefore, compared with algorithm depicted in section 5.3, wavelet transform has much lower orientation sensitivity.

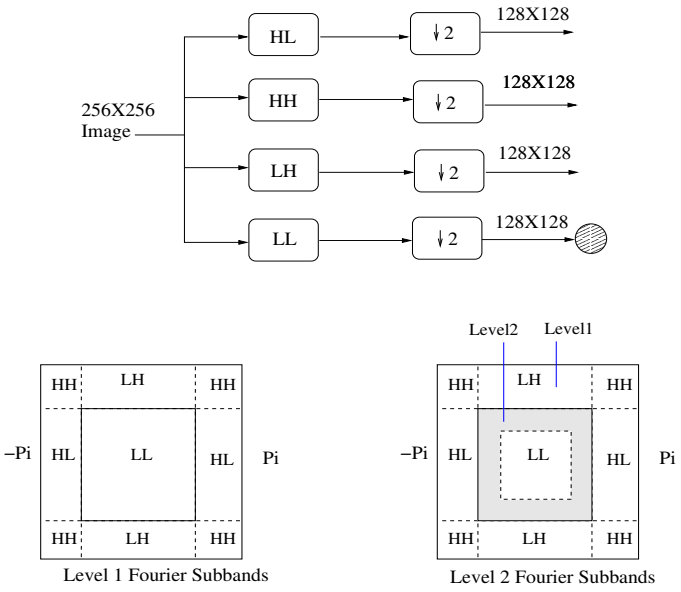


Figure 16: Top : Schematic diagram of wavelet pyramid. Bottom : Fourier domain partitioned by wavelets.Letter H and L represent High/Low-pass filter. The first letter represent filter for horizontal axis and the second letter represent filter fro vertical axis, e.g. HL represent highpass in x and lowpass in y.

### 5.5 Combine Orientation Information from all Scales

This section explains how to use state-space model to combine multiscale information [6]. The pyramidal structure of the orientation field can be defined on the quadtree structure, Figure 17 . Each node $\mathbf{t}$ is indexed as a triple $[m, i, j]$, where $m$ is the scale index, with $m = 1$ being the coarsest scale, and $i, j$ for the location. We define our multiscale orientation field as a set of orientation vectors indexed by scale and space, namely $Y(m, i, j)$. Also define $\bar{\mathbf{t}}$ be the parent of node $t$. Our model is,

$$\begin{aligned} \text{State Eq. } Y(\mathbf{t}) &= Y(\bar{\mathbf{t}}) + w(\mathbf{t}), \quad w(\mathbf{t}) \sim N(0, \sigma^2_{w_t}) \quad (6) \\ \text{Observation Eq. } X(\mathbf{t}) &= Y(\mathbf{t}) + v(\mathbf{t}), \quad v(\mathbf{t}) \sim N(0, \sigma^2_{v_t}) \quad (7) \end{aligned}$$

The state equation can be interpreted as that finer scales introduce additional detail $w(\mathbf{t})$ into the coarser signals. The observation equation quantify the uncertainty of the estimated value $X$ of node $t$. Let $m = m(\mathbf{t})$ be the scale of node $t$, we can rewrite the model as

$$\begin{aligned} \text{State Eq. } Y(m+1) &= Y(m) + w(m+1), \quad w(m) \sim N(0, \sigma^2_{w_m}) \quad (8) \\ \text{Observation Eq. } X(m) &= Y(m) + v(m), \quad v(m) \sim N(0, \sigma^2_{v_m}) \quad (9) \end{aligned}$$

And assume $p(Y_1^1) \sim N(X_1, \sigma^2_{v_1})$. Though, gaussian noise is not a correct model of directional data, both value of $w$ and $v$ are small and guassian is reasonable approximation.

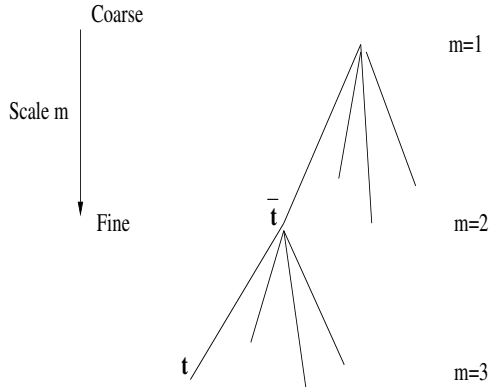


Figure 17: Quadtree from coarse to fine scale

Let $I(m) = \{x(1) \dots x(m)\}$

$$\begin{aligned} E(Y(m+1)|I(m+1)) &= E(Y(m+1)|I(m)) + K \times (X(m+1) - E(Y(m+1)|I(m)) \\ \hat{Y}^{m+1}_{m+1} &= \hat{Y}^m_{m+1} + K \times (X_{m+1} - \hat{Y}^m_{m+1}) \end{aligned}$$

K is Kalman gain, i.e.

$$K = \frac{var(\hat{y}^m_{m+1})}{var(\hat{y}^m_{m+1}) + var(v_m)}$$

$$= \frac{{\sigma^2}^m_{m+1}}{{\sigma^2}^m_{m+1} + \sigma^2_{v_m}} \tag{10}$$

**Proxy for the variance** In Eq(10), ${\sigma^2}^m_{m+1}$ is the uncertainty of the prediction of $Y(m+1)$ given observation up to scale $m$. And $\sigma^2_{v_m}$ is the uncertainty of the estimation of $Y(m)$. These quantities are unknown. Instead, I use the the inverse of strength of orientation as a proxy of the uncertainty measure. And Kalman gain can be approximated by

$$K \approx \frac{1/S_m}{1/S_m + 1/S_{m+1}} = \frac{S_{m+1}}{S_m + S_{m+1}}.$$

A justification of using $1/S$ as the proxy of uncertainty is as follows.

At point $\mathbf{u}$ of a image,let $w_{m,\theta}$ be the the coefficient of transform at level $m$ and angle $\theta$ (see Eq ), and $w^2_{m,\theta}$ be the energy of transform. Then,

$$S_m = \sum w^2_{m,\theta} \times \bar{R},$$

where

$$\bar{R} = \frac{\sum_\theta w^2_{m,\theta} e^{i2\theta}}{\sum_\theta w^2_{m,\theta}} = \sum_\theta \tilde{w}^2_{m,\theta} e^{i2\theta}.$$

From directional statistics [9], for a 2D Gaussian distributed random vector field, the direction of the vectors will have von Mises distribution, with the probability density function (pdf) :

$$f(\theta, \mu, k) = \frac{1}{2\pi I(k)} e^{k\cos(\theta-\mu)}$$

where

$$I(k) = \frac{1}{2\pi} \int_o^{2\pi} e^{k\cos(\theta)},$$

$\mu$ is mean direction and $k$ is concentration of the distribution. In orientation estimation, vectors and we can model such distribution using Bingham distribution. Given the pdf of von Mises distribution $f(\theta)$, the pdf of Bingham distribution $g(\theta) = f(2\theta)$. For small $k$ , $k \propto \bar{R}$. If we accept that the distribution of energy of signal at $\mathbf{u}$ is an approximation of distribution of our orientation estimate, $S_m$ is a good indicator of certainty of orientation estimation at level $m$. Since a high concentration of energy at level $m$ means higher value of $\sum_\theta w^2_{m,\theta}$, while $\bar{R}$ measure the concentration of energy at level $m$. Thus, $1/S_m$ a is reasonable measure of the uncertainty of our estimates.

### 5.6 Algorithm for Fitting Rectangle to the Center of Galaxy Image

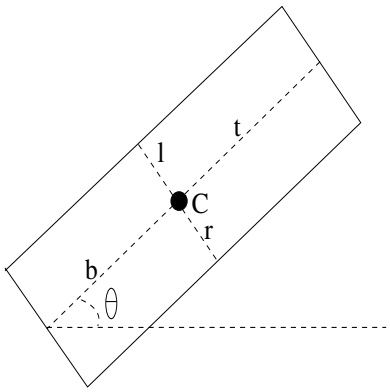


Figure 18:

Let $l, r, tb$ be the Edge-to-Center distance, Figure (18), $C$ be the center and $\theta$ be the orientation of the rectangle. For each point $\mathbf{p}$, let the loss function

$$\begin{aligned} L(\mathbf{p},\theta) &= -1, \quad |OrAng(\mathbf{p}) - \theta| < \pi/9 \quad \& \quad OrStr(\mathbf{p}) = 0 \\ &= 1, \quad \text{otherwise} \end{aligned}$$

where OrAng($\mathbf{p}$), OrStr($\mathbf{p}$) are orientation Angle and strength at point $\mathbf{p}$. $\pi/9$ is the maximum discretization error from the transform by the orienation flters.

Algorithm:

Initialization :

Input orientation field and estimated center $C$

Set $\theta$ be the orientation at $C$

l,r,t,b $\leftarrow 1$

Iteration:

for each edge {

if $\sum_{\mathbf{p}\in\text{edge}} L(\mathbf{p},\theta) < 0$

{

Increment Edge-to Center distance by 1

$\theta \leftarrow$ average orientation of all pixels within the current rectangle.

}

if (no increment for all edges)

stop

}

**Galaxy Evolution model with Cold Dark Matter**

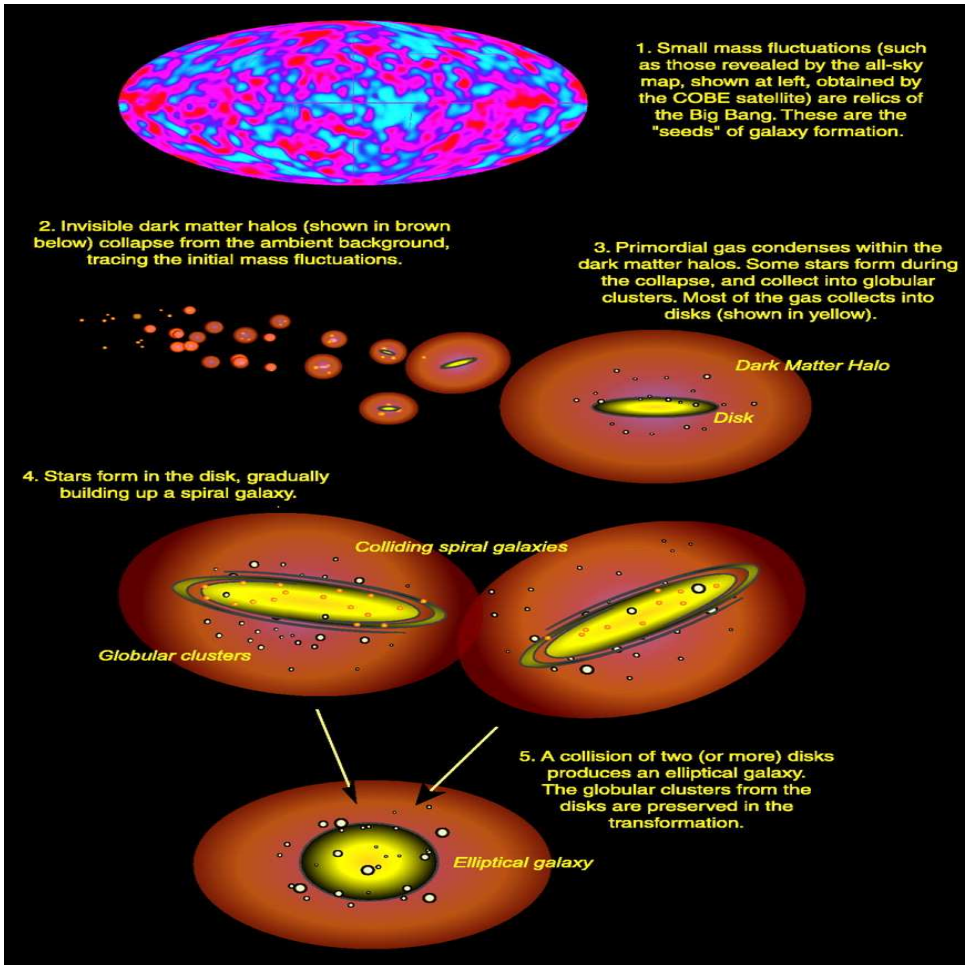


Figure 19: Schematic illustration of the formation of galaxies in the hierarchical formation model. It is worth noting that morphological transformations are cyclical in this model. Some elliptical galaxies formed by the collision of spirals will slowly accrete gas from the field, thus growing a new disk, and ultimately being transformed back into spiral galaxies with nuclear bulges. (Illustration from **Science** Vol293)

Since early 1980s, a new model for evolution of universe and galaxies is proposed which assume a large fraction of the universe is not in stellar or gaseous form, but is instead compose of dark matter. Dark matter does not emit or absorb radiation, and it can only be detected by its gravitational effects on galaxies. Theoretical work relies on the hypothesis that dark matter and galaxies are linked, because gravitating concentrations of dark matter originating soon after the Big Bang are responsible for the formation of galaxies. In this view, small concentrations of dark matter grow slowly at first, and are then gradually compressed by self-gravity. However, when the concentrations

reach a critical density, they undergo a catastrophic collapse, which results in the formation of an extended "halo" of dark matter. Over time these halos clump together under mutual gravitational attraction merging to form a hierarchy of larger halos. The rate of cooling and angular momentum of hydrogen gas drawn into these large halos governs the assembly of normal galaxies and their morphology (see figure 19).

Under this new model, galaxies are no longer viewed growing in isolation, but have active interaction with each others. By studying the relationship with abundance of each morphological types with its environment (like redshift and local density), we could have more clues about the history of the evolution process.e

### Bugle + Disk Decomposition

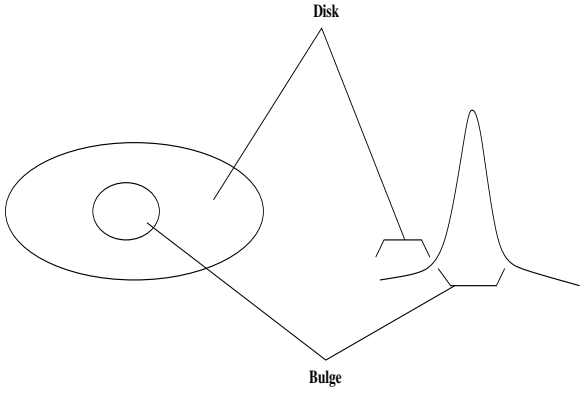


Figure 20: Schematic diagram of Bugle-Disk decomposition.

Figure 20 is a schematic diagram of Bugle-Disk decomposition. The left figure depicts a face-on diagram of a galaxy, the central part is the bugle and the peripheral part is the disk. The right figure is the a cross section of the surface brightness function of the galaxy;the bulge has higher brightness and gradient of brightness function, whereas the disk is dimer and has lower gradient of brightness function.

A two-dimensional surface brightness function for disk ($F_D$) and bugle ($F_B$) was fitted simultaneously to the observed intensity distribution. We can hence calculate the Bugle-to-Disk ratio

## Mexican Hat

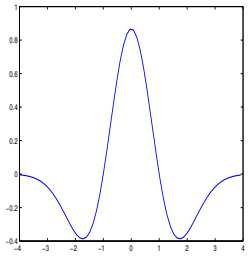

Figure 21: Mexican hat function

## 3D plot of eq 1 and 2

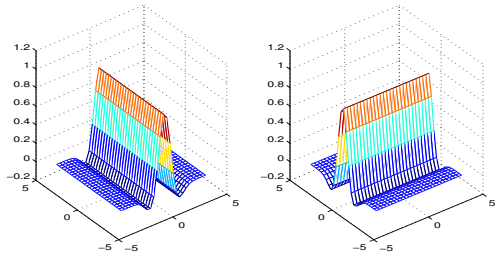

Figure 22: Plots of $\rho_\theta(x, y)$ at $\theta = 0, \pi/2$

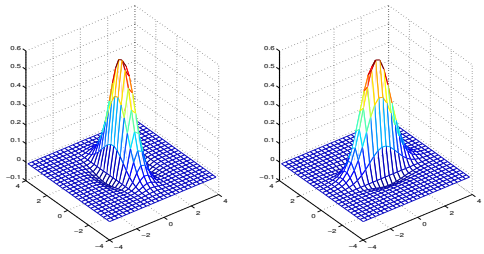

Figure 23: Plots of $\psi_\theta(x, y)$ at $\theta = 0, \pi/2$